THE JOURNAL OF PHYSICAL CHEMISTRY B

Article

pubs.acs.org/JPCB

Water Is a Poor Solvent for Densely Grafted Poly(ethylene oxide) Chains: A Conclusion Drawn from a Self-Consistent Field Theory-Based Analysis of Neutron Reflectivity and Surface Pressure−Area Isotherm Data

Hoyoung Lee,[†] Dae Hwan Kim,[†] Kevin N. Witte,[†] Kimberly Ohn,[†] Je Choi,[†] Bulent Akgun,[‡,§] Sushil Satija,[‡] and You-Yeon Won*[,†]

[†]School of Chemical Engineering, Purdue University, West Lafayette, Indiana, United States

[‡]NIST Center for Neutron Research (NCNR), National Institute of Standards and Technology (NIST), Gaithersburg, Maryland, United States

[§]Department of Materials Science and Engineering, University of Maryland, College Park, Maryland, United States

Supporting Information

ABSTRACT: By use of a combined experimental and theoretical approach, a model poly(ethylene oxide) (PEO) brush system, prepared by spreading a poly(ethylene oxide)−poly(*n*-butyl acrylate) (PEO−PnBA) amphiphilic diblock copolymer onto an air−water interface, was investigated. The polymer segment density profiles of the PEO brush in the direction normal to the air−water interface under various grafting density conditions were determined by using the neutron reflectivity (NR) measurement technique. To achieve a theoretically sound analysis of the reflectivity data, we used a data analysis method that utilizes the self-consistent field (SCF) theoretical modeling as a tool for predicting expected reflectivity results for comparison with the experimental data. Using this data analysis technique, we discovered that the effective Flory−Huggins interaction parameter of the PEO brush chains is significantly greater than that corresponding to the θ condition in Flory−Huggins solutions (i.e., $\chi_{PEO-water}$(brush chains)/$\chi_{PEO-water}$(θ condition) ≈ 1.2), suggesting that contrary to what is more commonly observed for PEO in normal situations ($\chi_{PEO-water}$(free chains)/$\chi_{PEO-water}$(θ condition) ≈ 0.92), the PEO chains are actually not "hydrophilic" when they exist as polymer brush chains, because of the many body interactions that are forced to be effective in the brush situation. This result is further supported by the fact that the surface pressures of the PEO brush calculated on the basis of the measured $\chi_{PEO-water}$ value are in close agreement with the experimental surface pressure−area isotherm data. The SCF theoretical analysis of the surface pressure behavior of the PEO brush also suggests that even though the grafted PEO chains experience a poor solvent environment, the PEO brush layer exhibits positive surface pressures, because the hydrophobicity of the PEO brush chains (which favors compression) is insufficient to overcome the opposing effect of the chain conformational entropy (which resists compression).

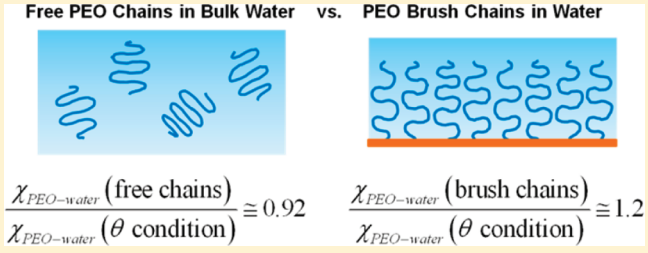

1. INTRODUCTION

Poly(ethylene oxide) (PEO) brushes are widely used for surface modification of biomaterials because the PEO chains can prevent the undesirable adsorption of proteins to the surfaces.[1,2] Interestingly, end-grafted PEO chains are often observed to form an unusually dense concentrated layer near the water−substrate interface.[3−6] A common explanation for this phenomenon has been that the (strong) hydrophobicity of the grafting surface (a situation frequently encountered in practice) causes the PEO segments to become highly accumulated toward the hydrophobic interface to shield the substrate material from unfavorable contacts with water molecules.[5,7]

In most previous discussions of the conformations of PEO brushes, however, there is one important aspect of the properties of PEO that is often ignored, which is the existence of many-body (attractive) interactions among the PEO segments; the hydration of PEO involves a configurational rearrangement of the polymer segments in coordination with the surrounding water molecules,[8,9] and therefore at high concentrations of PEO the specific configuration of the polymer that enables hydrophilic interaction with water may become disrupted, rendering the polymer less (or in)soluble in water. This many-body effect is well supported by experimental evidence of, for instance, an increase in the measured value of the effective Flory−Huggins interaction parameter ($\chi_{PEO-water}$),[10,11] and the formation of aggregates of PEO chains,[12] in bulk solution at elevated

Received: February 23, 2012
Revised: May 21, 2012
Published: May 22, 2012

concentrations of PEO. De Gennes and co-workers have incorporated this notion into a theoretical description of a polymer brush system (often referred to as the "n-cluster" theory) and predicted that a PEO brush can, in fact, form a collapsed structure even if the grafting surface is not hydrophobic.[13−15] There have been two reports of experimental observations in the literature that unambiguously, in our opinion, support the existence of this *n*-cluster effect in PEO brush systems. The first example is the study of Wu et al. in which it was found that the thickness of a PEO brush (grafted onto a poly(*N*-isopropylacrylamide) surface) becomes significantly reduced when the grafting density is increased above a certain threshold.[16] Recently, Davis et al. observed that the interaction between adamantine (AD) and cyclodextrin (CD) becomes strengthened by a few fold when their complexation occurs in the form of a reaction between AD-end-functionalized PEO chains and a nanoparticle surface-functionalized with CD moieties;[17] the many-body attractive interaction between the PEO brush chains appears to contribute to a further stabilization of the inclusion complex formed between the AD and CD functional groups. In both the cases, the PEO chains, when examined in the ungrafted state, were shown to have no tendency to adsorb to the grafting interfaces.

This line of thinking, however, raises a question: Why are, then, PEO brush coatings in water in general so effective in preventing aggregation of the coated particles (rather than causing the aggregation due to the hydrophobicity of the PEO brush chains)? We believe that the answer to this question lies in the answer to another: How hydrophobic would PEO chains become when they exist as polymer brush chains? To our knowledge, there has not previously been an attempt to determine the value of the $\chi_{PEO-water}$ parameter for PEO chains in the polymer brush conformation. This is what the present study attempted to do.

In this work, we use an air−water interfacial monolayer formed from a poly(ethylene oxide)-poly(*n*-butyl acrylate) (PEO−PnBA) diblock copolymer as a model system to study the conformational and thermodynamic properties of the PEO brush chains. As will be discussed in sections 3.1 and 3.2, the PnBA material has a unique combination of interfacial properties such that the polymer completely wets the air−water interface, and thus forms a flat continuous water-free single-monomer-thick interfacial film at high surface polymer concentrations. Also, PEO chains dissolved in water were found to have no tendency to adsorb to the PnBA−water interface (section 3.1). These properties of PnBA make this polymer uniquely suited as the anchoring block chemistry for preparation of a model non-adsorbing PEO brush system. We would also like to point out that there are a couple of advantageous aspects to using PEO brushes grafted at the air−water interface (rather than the solid−water interfaces). The first is that using the air−water interfacial system facilitates precise and continuous control of the interfacial area per chain of the brush, which is an important parameter that determines many properties of the system. Also, the surface pressure caused by the lateral interchain interactions in the brush layer can be readily measured as a function of monolayer area by using the Langmuir film balance technique, which will provide useful data for comparison and validation of other measurements (as will be demonstrated in section 3.4). These surface pressure measurements will also allow us to obtain an answer to another important related question (also pointed out earlier by Halperin):[14] *If indeed the grafted PEO chains experience an unfavorable solvent environment due to the n-cluster effect, would the brush layer favor lateral compression and exhibit negative surface pressures?* (Results concerning this problem will be discussed in section 3.4.)

The conformations of the grafted PEO chains were probed by neutron reflectivity (NR). These NR data were quantitatively compared to theoretical reflectivity profiles calculated on the basis of a sophisticated self-consistent field (SCF) theory (section 3.3). We found that the experimental data can be quantitatively fit by the theoretical model when the $\chi_{PEO-water}$ parameter is set to a value close to 0.8. This result unarguably suggests that PEO chains indeed experience a poor solvent environment when they exist as polymer brush chains. Further, at the best-fit $\chi_{PEO-water}$ condition, the values of the surface pressure produced by the lateral interactions between the PEO brush chains were calculated for varying PEO grafting densities using the SCF theory-based model. The results of these calculations show a good agreement with the experimental surface pressure−area isotherm data, supporting the validity of the results obtained from the analysis of the NR data (section 3.4).

2. EXPERIMENTAL PROCEDURES

2.1. Polymer Samples. The poly(ethylene oxide) (PEO) homopolymer material used in this study was monomethoxy and monohydroxy-terminated PEO. This polymer was purchased from Polysciences, Inc. (Warrington, PA). Its molecular characteristics are DP_n (number-average degree of polymerization) = 113 (determined by ^{1}H NMR) and PDI (polydispersity index) = 1.07 (determined by gel permeation chromatography (GPC) using a molecular weight calibration based on polystyrene standards). The poly(*n*-butyl acrylate) (PnBA) homopolymer and PEO−PnBA diblock copolymer samples were synthesized and characterized as described in our previous publications.[18−21] The molecular characteristics of the PnBA homopolymer are DP_n = 102 (determined by ^{1}H NMR) and PDI = 1.12 (determined by GPC). The molecular characteristics of the PEO−PnBA diblock copolymer are $DP_{n,PEO}$ = 113 (determined by ^{1}H NMR), $DP_{n,PnBA}$ = 100 (determined by ^{1}H NMR), and PDI (for the overall molecular weight distribution) = 1.28 (determined by GPC).

2.2. Surface Pressure−Area Isotherm Measurements. Surface pressure−area isotherms were collected using a KSV 5000 Langmuir trough (15.0 cm × 51.0 cm × 1.0 cm) within a plexiglass chamber. The hydrophobic trough and hydrophilic symmetric moving barriers were cleaned by repeated rinsing with ethanol followed by deionized water. The surface pressure was measured by the Wilhelmy method using a platinum plate, located equidistant from each barrier, which was cleaned by rinsing with ethanol and water and then flamed. Deionized Millipore water (18 MΩ·cm resistivity) was used as the substrate, the surface of which was cleaned via aspiration prior to spreading. The cleanliness of the surface and probe were checked by compressing the water surface at 3 mm/min and monitoring the surface pressure. If the total change in the pressure was greater than 0.2 mN/m, the surface and probe were recleaned and measurement retaken until the surface pressure change was below this threshold. Polymer solutions in chloroform were prepared in clean, dust-free glass vials. These vials were tightly sealed with Parafilm and stored at −20 °C prior to use. For a measurement, a designated quantity of the polymer solution was spread dropwise on the water surface using a Hamilton microsyringe. The surface pressure was monitored after spreading until it was stabilized to a constant value, typically 3−4 h. The isotherm was then recorded while compressing the

dx.doi.org/10.1021/jp301817e | J. Phys. Chem. B 2012, 116, 7367−7378

barriers at 3 mm/min. All isotherm data presented in this paper were reproducible for independent repeated trials to within 1% variation in the surface pressure (Π) or area per chain (α) values.

2.3. Neutron Reflectivity (NR) Experiments. NR measurements were conducted on the NG7 Horizontal Neutron Reflectometer at the National Institute of Standard and Technology (NIST) Center for Neutron Research (NCNR) in Gaithersburg, MD. The PEO–PnBA monolayer was prepared on a Langmuir trough (70 mm × 70 mm × 2 mm, made of Teflon) containing a separate pocket (25 mm × 25 mm × 3 mm) for a Wilhelmy plate. The trough was equipped with a movable single barrier (5 mm × 12 mm × 80 mm, also made of Teflon). In all NR experiments, heavy water (D_2O) was used as the subphase on which the monolayer was spread. The D_2O compound used was purchased from Cambridge Isotope Laboratories, Inc. (D, 99.8%) and was used as received. The specular reflectivities were measured using an unpolarized incident neutron beam at a wavelength (λ) of 4.760 Å. The reflected intensities were measured in the range of out-of-plane momentum transfer vector (q_z) from 0.012 $Å^{-1}$ to 0.23 $Å^{-1}$; the momentum transfer vector is related to the angle of reflection (θ) by $q_z = (4\pi/\lambda) \sin\theta$. For different reflection angles, the angular divergence of the incident neutron beam was adjusted so that the q_z resolution is kept roughly constant around an optimum level of $\Delta q_z/q_z = 0.04$ across the measurement q_z range. All measurements were conducted at room temperature. The raw data were reduced using the REFLPAK software suite from NCNR.[22] Off-specular contributions to the measured reflectivities were subtracted from the raw data.

2.4. National Institute of Standards and Technology (NIST) Disclaimer. Commercial materials, instruments, and equipment are identified in this paper to specify the experimental procedure as completely as possible. In no case such identification imply a recommendation or endorsement by the NIST nor does it imply that the materials, instruments, or equipment identified are necessarily the best available for the purpose.

3. RESULTS AND DISCUSSION

3.1. Poly(ethylene oxide) (PEO) Segments Do Not Adsorb to the Air–Water Interfacial Monolayer of Poly(*n*-butyl acrylate) (PnBA). As discussed in the Introduction, a common explanation for the collapsed conformation of the end-grafted PEO chains has been that the accumulation of the PEO segments toward the grafting surface occurs because of the strong hydrophobicity of the grafting surface; the collapsed brush structure provides a shielding of the hydrophobic surface from unfavorable contact with water molecules.[7] However, as reviewed in the Introduction, the *n*-cluster theory of de Gennes[15,23] suggests that a PEO brush may exist in a similar collapsed conformation regardless of whether the grafting surface is strongly hydrophobic. To experimentally test the role (or the lack) of the surface hydrophobicity in causing the brush chains to collapse, in the present work, we used a model PEO brush system in which the grafting surface itself does not provide any driving force for the PEO segments to adsorb onto it. Specifically, a Langmuir monolayer was prepared from a PEO–PnBA diblock copolymer; when sufficiently (laterally) compressed, the PnBA blocks form a laterally uniform, water-free monolayer, and the hydrated PEO chains, end-grafted to the PnBA film, form a brush layer. We feel that before discussing the properties of the PEO–PnBA monolayer, it is necessary to discuss those of the individual component polymers. For this reason, in the present subsection, we will present a discussion of the air–water interfacial properties of PnBA homopolymers and their interactions with free PEO chains dissolved in the subphase solution.

In a previous publication, we have reported results of an extensive study (including surface pressure–area, Brewster angle microscopy, and X-ray reflectivity measurements) for films of PnBA homopolymers spread on water.[21] The relevant findings of the study can be summarized as follows. As demonstrated in Figure 1A, a typical surface pressure (Π) vs area per chain (α) isotherm of a PnBA polymer exhibits a sharp transition upon compression from a compressible fluid state to a plateau of surface pressure (for instance, in the case demonstrated in the figure (DP_n = 102), the transition occurs at an area per chain value of α_o = 2120 $Å^2$/chain). This transition corresponds to a point where the air–water interface becomes fully covered with a single-monomer-thick, continuous (water-free) monolayer of PnBA, and further compression beyond this point causes the monolayer to form small (micrometer-sized) domains of collapsed PnBA aggregates; the number of, and the area occupied by, such domains are, however, quite negligible (for example, at $\alpha = 0.63 \cdot \alpha_o$, the collapsed domains occupy only 2% of the total monolayer area). An important characteristic of PnBA that makes the polymer uniquely suited for use as the anchoring block chemistry is that this polymer has a strong tendency to wet and spread over the air–water interface, as indicated by a large positive value of the polymer's spreading coefficient, s ($\equiv \gamma_{air-water} - \gamma_{PnBA-air} - \gamma_{PnBA-water}$) ≈ 21 mJ/$m^2$ at room temperature.[24] Unlike other hydrophobic polymers (such as polystyrene[25,26])

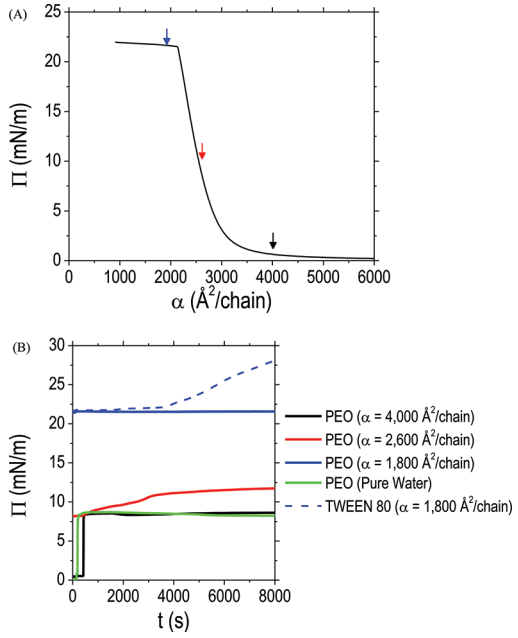

Figure 1. (A) Surface pressure (Π) vs area per chain (α) isotherm for an air–water interfacial monolayer of the PnBA homopolymer (DP_n = 102). (B) Changes in Π recorded as a function of time (t) after injection of PEO (at t = 100 s) into the subphase of the PnBA monolayer compressed to three different area per chain values (marked with arrows in (A)): α = 4000 (black), 2600 (red), and 1800 (blue) $Å^2$/chain. Also shown for comparison are two additional Π vs t curves, one obtained after injection of PEO (DP_n = 113) into pure water with no PnBA prespread on it (green) and another obtained by an injection of Tween 80 surfactant into the subphase of the PnBA monolayer at α = 1800 $Å^2$/chain (broken line).

dx.doi.org/10.1021/jp301817e | J. Phys. Chem. B 2012, 116, 7367–7378

that dewet and form small aggregates at the air−water interface, the PnBA segments of PEO−PnBA block copolymers form a molecularly flat air−water interfacial film onto which the PEO chains are end-grafted, and therefore the PEO−PnBA monolayer can serve as a convenient model system to study the conformations of the end-grafted PEO chains. Further, the low glass transition temperature (T_g) of the PnBA material (≈−55 °C)[27] allows us to control, continuously and reversibly, the grafting density of the PEO brush.

In our previous work, the static contact angle of a water droplet placed on a spin-coated PnBA surface was measured to be 84.2 ± 3.8°;[21] note that the contact angle was less than 90°, even though the bulk PnBA material used was found to be completely insoluble in water. This result suggests that the exposed surface of a bulk PnBA material is actually not very hydrophobic possibly due to the rearrangement of the side chain conformation, i.e., perhaps not hydrophobic enough to induce a collapse of the PEO chains tethered to it. To confirm this point, we conducted the following experiments; first, a PnBA homopolymer (DP_n = 102) was spread on a large area of water and then compressed to a certain designated α value; subsequently, a small volume of a water solution containing a known concentration of PEO homopolymer (DP_n = 113) was injected into the subphase of the monolayer (to a final PEO concentration in the subphase solution of about 50 mg/L); afterward, the change in Π was recorded as a function of time with a platinum Wilhelmy plate. The results are shown in Figure 1B. In this study, we hypothesized that adsorption of the PEO chains onto the PnBA monolayer would cause a change in the surface pressure of the monolayer. To verify this hypothesis, we conducted a control experiment in which the PnBA monolayer was initially compressed to an area of α = 1800 Å^2 per molecule, and nonionic Tween 80 surfactant (also called polysorbate 80 or polyoxyethylene(80) sorbitan monooleate) was then injected into the subphase to a concentration of 10 μM. The result of this control experiment is also displayed in Figure 1B (shown in broken line). As shown in the figure, the surfactant adsorption causes a gradual increase in monolayer pressure. On the basis of our previous finding that the plateau pressure in the collapsed full coverage regime (i.e., when $\alpha < \alpha_o$) is equal to the surface (free) energy change (per area) associated with removal of the PnBA monolayer from the air−water interface (i.e., $\Pi_o = \gamma_{air-water} - \gamma_{PnBA-air} - \gamma_{PnBA-water}$),[24,28] the surface pressure increase observed after the Tween 80 injection can be interpreted as being caused by a decrease in the $\gamma_{PnBA-water}$ quantity due to the adsorption of Tween 80 molecules on the water side of the PnBA monolayer.

Actual PEO adsorption experiments were conducted at three different area conditions; as indicated with arrows in Figure 1A, the three area per chain conditions examined were α = (i) 1800 Å^2/chain (marked with blue arrow), (ii) 2600 Å^2/chain (red arrow), and (iii) 4000 Å^2/chain (black arrow). The resultant surface pressure (Π) vs time (t) curves are presented in Figure 1B. At α = 4000 Å^2/chain, the monolayer pressure was found to increase rapidly upon injection of PEO (injected at a time corresponding to the 100 s point in the abscissa of the figure) from 0.5 to 8 mN/m (data shown in black) because of an adsorption of the PEO segments to the areas of the water surface that had not been coated with the prespread PnBA molecules; the adsorption behavior of PEO at the air−water interface has previously been reported,[29] and we have also included in Figure 1B a Π vs t curve obtained after injection of PEO into pure water with no PnBA prespread on it (shown in green), which is quite similar to the curve obtained in the presence of the spread PnBA molecules at the area per chain value of α = 4000 Å^2/chain. When the same amount of PEO was injected to the subphase of the PnBA monolayer at a monolayer area of α = 2600 Å^2 per chain (note that this area value is still slightly larger than the α_o value), the surface pressure was seen to increase only by a much smaller amount of ΔΠ ≈ 3.5 mN/m (i.e., initially from 8.2 to 11.7 mN/m) (red curve in Figure 1B), which is understandable because at this area per chain condition only a small portion of the original air−water interfacial area remains uncoated by PnBA and is available for adsorption of the PEO chains. It is noted that the smaller number of adsorption sites for PEO is also reflected in the longer time it took for the adsorption process to reach equilibrium at α = 2600 Å^2/chain than in the α = 4000 Å^2/chain case. At α = 1800 Å^2/chain where the air−water interface was completely covered by PnBA (i.e., $\alpha < \alpha_o$), the injection of PEO did not produce any change in monolayer pressure, as shown with the solid blue curve (recorded over a 8000 s period) in Figure 1B. This result supports the hypothesis, introduced at the beginning of this section, that PEO does not have (at least, not as strong) a tendency to adsorb to a PnBA−water interface (as it does toward the air−water interface). Later in section 3.3, this nonattractive quality of the water-mediated interactions between PEO and PnBA segments will be confirmed again through the analysis of the neutron reflectivity (NR) data obtained from a PEO−PnBA diblock copolymer monolayer prepared at the air−water interface.

3.2. Surface Pressure−Area Isotherm Behavior of a PEO−PnBA Diblock Copolymer. In the present study, we used a PEO−PnBA diblock copolymer having molecular weights for the individual blocks of $DP_{n,PEO}$ = 113 and $DP_{n,PnBA}$ = 100. Before focusing our discussion on the properties of the PEO segments in the brush regime (section 3.3), in this section we present an overview of the conformational behavior of this diblock copolymer at the air−water interface at various regimes of surface polymer concentration as inferred from the Π−α isotherm of the copolymer; the diblock isotherm is presented in Figure 2A, along with the isotherm curve of the PnBA homopolymer (DP_n = 102) replotted from Figure 1A for direct comparison. We point out that the PEO−PnBA isotherm presented in the figure represents a composite of two separate measurements on two different ranges of surface area, and the complete match between the two data sets confirms the quantitative accuracy of the measurements. Through comparison with the homopolymer data, we were able to conclude about the molecular origins of the various transitions (i.e., plateaus and kinks) observed in the PEO−PnBA isotherm, as discussed below.

First, it should be noted that the isotherm curve of the diblock monolayer shows a very distinct transition upon compression from a fluid phase to a plateau of surface pressure (at an area per chain value of α_o = 2190 Å^2/chain) that is almost identical (in shape and lateral position) to that observed in the homopolymer data; as discussed in the previous section, in the PnBA homopolymer case (DP_n = 102) this plateau transition occurs at α_o = 2120 Å^2/chain, which gives a value of 21 Å^2/chain for the area occupied by a PnBA monomer at the transition point. In the diblock situation ($DP_{n,PnBA}$ = 100), the same calculation gives an essentially indistinguishable value of 22 Å^2 per PnBA monomer for the same parameter. This analysis indicates that the nature of the plateau transition in the PEO−PnBA curve is identical to what was concluded in the previous section for the PnBA homopolymer; the transition point is the point where the water surface becomes fully covered with a single-monomer-thick

dx.doi.org/10.1021/jp301817e | J. Phys. Chem. B 2012, 116, 7367−7378

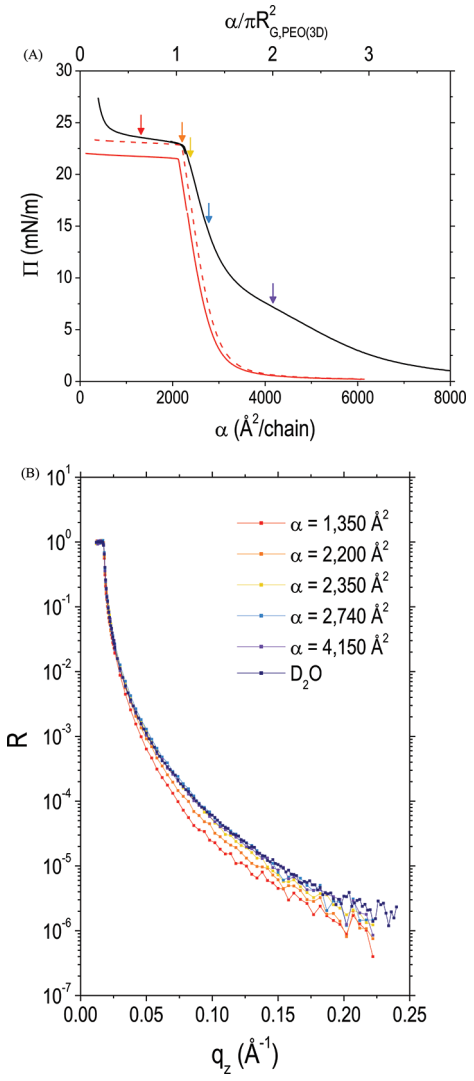

Figure 2. (A) Surface pressure (Π) vs area per chain (α) isotherm for the PEO−PnBA diblock copolymer ($DP_{n,PEO}$ = 113, and $DP_{n,PnBA}$ = 100) (black line). Also shown for comparison are the isotherm curve of the PnBA homopolymer (DP_n = 102) replotted from Figure 1A (red solid line) and a rescaled plot of the homopolymer isotherm produced by first adding a constant (=72 Å^2/chain) to the area/chain values of the original homopolymer isotherm to make the critical area equal to that observed for the PEO−PnBA and then multiplying the surface pressure values of this shifted homopolymer isotherm further by a constant factor (=1.06) to make its plateau pressure at the full-coverage transition identical to that of the diblock isotherm (red dashed line). (B) Neutron reflectivity (NR) profiles from the PEO−PnBA monolayer at five different α conditions denoted using arrows in (A). Displayed for comparison is the NR profile of the air−D_2O interface.

monolayer of pure PnBA. We would also like to note that in previous publications[24,28] we have also shown that the surface pressure−area behavior of a different PnBA-based diblock copolymer, poly(2-(dimethylamino)ethyl methacrylate)−poly(*n*-butyl acrylate) (PDMAEMA-PnBA, $DP_{n,PDMAEMA}$ = 80 and $DP_{n,PnBA}$ = 94), undergoes the plateau transition at a monolayer area of α_o = 2000 Å^2 per chain, which again gives essentially the same value of 21 Å^2 for the area of a PnBA monomer at the transition point (further supporting the above explanation).

Another important aspect of the difference between the copolymer and homopolymer isotherms is that the PEO−PnBA isotherm curve shows a considerably higher plateau pressure (Π_o = 22.8 mN/m at the full-coverage transition) than the isotherm of PnBA (Π_o = 21.5 mN/m at the full-coverage transition). As discussed in section 3.1, the plateau value of the surface pressure represents the cost in surface tension for removal of the PnBA monolayer from the air−water interface ($\Pi_o = \gamma_{air-water} - \gamma_{PnBA-air} - \gamma_{PnBA-water}$). Under this model, the higher plateau pressure observed for the diblock monolayer can be understood as a result of a decrease in $\gamma_{PnBA-water}$ caused by the presence of the chemically grafted PEO chains at the PnBA−water interface. A similar effect has also been observed in the isotherm of a PDMAEMA-PnBA monolayer (Π_o = 22.5 mN/m at the full-coverage transition).[28]

Further compression beyond the onset of full surface coverage (i.e., to an area per chain $\alpha < \alpha_o$) causes a collapse of the spread PnBA chains into three-dimensional structures. As mentioned in the previous section, in a monolayer formed by a PnBA homopolymer, this monolayer collapse leads to formation of micrometer-scale aggregates ("domains").[21] To test whether the same happens in the PEO−PnBA monolayer, the lateral uniformity of the monolayer film was examined at an area per chain condition of α = 2000 Å^2/chain by atomic force microscopy (AFM). The resultant image is presented in Figure S1 of the Supporting Information (SI). As shown in the figure (unlike what was found for the PnBA homopolymer), the diblock copolymer film was found to be laterally uniform at the area condition examined within the resolution of the AFM technique; in the diblock case, we believe, the chemical linkage between the PEO and PnBA blocks prohibits the collapsed PnBA segments from aggregating into large domains. This lateral microscopic homogeneity is thought to be a unique property of the PEO−PnBA monolayer, one that makes it ideal as a model system to study the conformational properties of the PEO brush chains.

In the range $\alpha > \alpha_o$ where there exist open areas of water surface uncovered by the polymer, the PEO−PnBA isotherm becomes significantly different from that of PnBA; as shown in Figure 2A, the magnitude of this discrepancy is clearly visualized when the diblock isotherm is compared with a rescaled plot of the homopolymer isotherm (shown with a dashed line in the figure) that has been produced by first adding a constant (=72 Å^2/chain) to the area/chain values of the original homopolymer isotherm to make the critical area equal to that observed for the PEO−PnBA (this procedure is to correct for the difference in the PnBA molecular weight) and then multiplying the surface pressure values of this shifted homopolymer isotherm further by a constant factor (=1.06) to make its plateau pressure at the full-coverage transition identical to that of the diblock isotherm (to account for the difference in $\gamma_{PnBA-water}$).[28] The higher surface pressures exhibited by the PEO−PnBA monolayer throughout the partial coverage regime is believed to be a consequence of strong adsorption of the PEO segments to the air−water interface. It is interesting to note that this behavior of PEO−PnBA is in contrast to what has been observed in studies of PDMAEMA−PnBA films where the brush-forming PDMAEMA chains do not have a preference to locate at the air−water interface (see Figure 5 in ref 28).

We also note that a small humplike feature (or "pseudo-plateau") was seen in the PEO−PnBA isotherm in the $\alpha \approx$ 3000−6000 Å^2 per chain range. In the present work, we did not intend to investigate in full detail the conformational behavior of the block copolymer in this precollapse regime. Nevertheless, below we present a simple analysis that helps speculate what changes in molecular conformation might be responsible for the pseudoplateau behavior observed. In a previous publication,[21] we

dx.doi.org/10.1021/jp301817e | J. Phys. Chem. B 2012, 116, 7367−7378

have shown that a PnBA chain spread on a water surface assumes a two-dimensional (2D) swollen coil conformation with a characteristic Flory exponent for the 2D radius of gyration of approximately 0.57. In the literature, it has been reported that the energy of adsorption of a PEO monomer to the air−water interface is estimated to be about $-k_BT$,[30] and therefore it is reasonable to assume that an isolated PEO chain is expected to adopt a flat 2D conformation at the air−water interface. Assuming, for these reasons and for simplicity, that the spread PEO−PnBA diblock chains at sufficiently low surface concentrations assume a 2D Gaussian coil structure, the radii of gyration of the individual blocks can be estimated as $R_{G,PEO}^2 = DP_{PEO}\cdot b_{PEO}^2/4$ and $R_{G,PnBA}^2 = DP_{PnBA}\cdot b_{PnBA}^2/4$ (the values of the statistical segment lengths for PEO and PnBA have been found to be b_{PEO} = 5.9 Å[31] and b_{PnBA} = 7.0 Å (based on parameters for poly(ethyl acrylate))[32]).[33] Thus, (the minimum likelihood estimate of) the overall radius of gyration for the copolymer can be calculated using the relation $R_{G,PEO-PnBA}^2 = R_{G,PEO}^2 + R_{G,PnBA}^2$;[31] the actual value of this $R_{G,PEO-PnBA}$ quantity was estimated to be 47.1 Å. Therefore, the 2D chain-overlap condition (at which the pervasive areas of the isolated diblock chains begin to interpenetrate) is estimated to be α^* $(=\pi R_{G,PEO-PnBA}^2) \approx 7000$ Å^2/chain. This estimated value for the chain-overlap area (α^*) exceeds, within a factor of order unity, the value of α at the onset of the pseudoplateau (≈4500 Å^2/chain), which supports that the plateau-like behavior of surface pressure may be an indication of a conformational transition of the PEO segment from a surface-bound state to a water-submerged structure, similar to what has been predicted for homopolymers moderately adsorbed to an air−liquid interface upon an increase of the surface concentration (termed a "pancake-to-cigar" transition).[34]

Lastly, we point out that in the collapsed regime (i.e., at $\alpha < \alpha_o$), the PEO−PnBA monolayer was seen to be more resistant to compression than the simple PnBA film (that is, $\Pi_{PEO-PnBA} > \Pi_{PnBA(rescaled)}$); as will be discussed in quantitative detail in section 3.4, in this area per chain region, the lateral repulsion between the PEO chains produces a significant rise in monolayer pressure. This result is also consistent with the fact that in this regime, the normalized area per chain value, $\alpha/\pi R_{G,PEO(3D)}^2$, is less than unity (as shown on the second x-axis of Figure 2A); here, $R_{G,PEO(3D)}$ is the radius of gyration of the PEO block in the three-dimensional self-avoiding random-walk configuration, and its value (≈25.7 Å) was estimated using parameter values reported in ref 35. Therefore, when $\alpha < \alpha_o$, the end-grafted PEO chains are truly in the "brush" configuration; a more detailed discussion of this issue has been presented elsewhere.[36] In the remainder of this paper, we will focus discussion on the behavior of the PEO chains in this polymer brush regime.

3.3. Neutron Reflectivity (NR) Study of the PEO Brush Formed at the Air−Water Interface. The conformation of the PEO brush formed by the PEO−PnBA diblock copolymer ($DP_{n,PEO}$ = 113, and $DP_{n,PnBA}$ = 100) at the air−water interface was investigated by using the neutron reflectivity (NR) technique. To demonstrate that the PEO segments submerged in the D_2O subphase give rise to a sufficient NR signal, we display, in Figure 2B, the NR profiles obtained from the PEO−PnBA monolayer at the five different α conditions indicated with arrows in Figure 2A. Also shown for comparison in Figure 2B is the NR profile obtained from a surface of pure D_2O. It can be seen from the figure that in the (out-of-plane) momentum transfer vector range accessible with the NR technique ($q_z < 0.25$ Å^{-1}), the NR curves for the PEO−PnBA diblock copolymer show a significant deviation from the NR profile of the air−D_2O interface and also significant variations with changes in α, which confirms that the NR measurements are sufficiently sensitive to probe for the conformations of the end-grafted PEO chains and to detect changes in their conformations under varying values of α.

As has been reported elsewhere, we have also performed X-ray reflectivity (XR) measurements on the same PEO brush system. In the present study, the NR results shown in Figure 2B (rather than the previous XR data) were analyzed to determine the value of the $\chi_{PEO-water}$ parameter. This was for two reasons. First, the NR technique is more sensitive to the brush features. This point can be shown by comparing, between the neutron and X-ray scattering methods, the values of the scattering contrast of PEO against water; for neutron scattering, $(SLD_{D_2O} - SLD_{PEO})/SLD_{D_2O}$, ≈0.89 (where SLD_i denotes the scattering length density of species i, and the SLD values for the individual species are listed in Table 1), whereas for X-ray scattering, $(\rho_{e,PEO} - \rho_{e,H_2O})/\rho_{e,H_2O} \approx 0.22$ (where $\rho_{e,i}$ denotes the electron density of i, and the ρ_e data are also given in Table 1). The second reason has to do with the fact that for an estimation of $\chi_{PEO-water}$, the reflectivity data need to be analyzed within a polymer brush theory. In the previous XR study, it was found that the density of water inside the PEO brush (in particular, in the region close to the PnBA−water interface) is lower than its bulk value by about 5%.[36] In the NR case, the effect of this water rarefaction causes only a minor contribution to the overall reflectivity behavior of the PEO brush; the change in the water contrast factor due to the ∼5% decrease in water density amounts to a small fraction of the scattering contrast between PEO and D_2O (i.e., 5% of $SLD_{D_2O}/(SLD_{D_2O} - SLD_{PEO}) \approx 0.056$). This fact allows us to ignore the water rarefaction effect in the theory-based analysis of the NR results. The same is not true for the XR situation, as can be seen from the calculation, 5% of $\rho_{e,H_2O}/(\rho_{e,PEO} - \rho_{e,H_2O}) \approx 0.229$.

Table 1. Neutron Scattering Length Density (SLD) and Electron Density (ρ_e) Values of Heavy Water (D_2O), Poly(ethylene oxide) (PEO), and Poly(*n*-butyl acrylate) (PnBA)[a]

species	mass density (g/cm^3)	SLD (10^{-6} Å^{-2})	electron density (e$^-$/Å^{-2})
H_2O	0.9970	−0.5582	0.33328
D_2O	1.1056	6.3607	0.33243
PEO	1.239[49]	0.7011	0.40610
PnBA	1.101[36]	0.6859	0.36166

[a]The bound coherent scattering lengths for hydrogen (H), deuterium (D), carbon (C), and oxygen (O) atoms are b_H = −3.739 fm, b_D = 6.671 fm, b_C = 6.646 fm, and b_O = 5.803 fm, respectively.[48]

The NR profiles of the PEO−PnBA monolayer are characterized by a lack of any oscillatory features (such as the ones reported in ref 37); the reflectivity monotonically decays with increasing q_z. This result suggests that the end-grafted PEO chains form a diffuse layer that smoothly extends some distance into the subphase solution without formation of any dense collapsed sublayer, which is consistent with the above-discussed argument that PEO does not have a tendency to adsorb to the PnBA−water interface (section 3.1). Another important trend observed in the diblock results is that the high-q_z intensities decrease with increasing surface polymer concentration (i.e., with decreasing α). This result can be understood by the fact that

dx.doi.org/10.1021/jp301817e | J. Phys. Chem. B 2012, 116, 7367−7378

as α is decreased, the PEO chains become more stretched from the grafting surface due to increased overlap between adjacent chains, and thus the PEO segment distribution becomes more diffuse toward the subphase, which gives rise to a more rapidly decaying reflectivity profile; this interdependence between the interfacial diffuseness and the reflectivity pattern is easily deducible from, for example, the simple kinematic formalism of reflectivity for a rough interface.[38]

For analysis of the NR data for the PEO brush, we used an approach that uses a numerical self-consistent field (SCF) theory as a tool to produce predictions for expected reflectivity results for comparison with the experimental data. In most previous NR/XR studies, reflectivity data from block copolymer monolayers at the air−water interface have been modeled with the so-called multiple-box model (in which the scattering volume is divided into a finite number of horizontal sublayers of distinct scattering length/electron densities with smeared interfaces between adjacent sublayers). In this approach, the outcome of the fitting is simply the overall scattering length/electron density profiles that are weighted superpositions of the density profiles of the individual block copolymer components. Therefore, this box-model approach is not capable of separately determining the segment density distributions of the individual blocks, nor (more importantly) capable of providing information about the underlying thermodynamic causes of the observed chain conformations. In the present study, to be able to establish a theoretically based understanding of experimental NR results, it was necessary to incorporate the SCF theory into the analysis of the experimental data. Also, we point out that there are a couple of additional (technical) advantages of the approach developed in the present study; in fitting to experimental data, we can restrict our search for the best-fit model to the subset of polymer conformations that are physically feasible and that satisfy the overall mass balance constraint, which makes the analysis process more rationally based and efficient overall. We note that during the revision of this article we became aware of the work by Zhang et al. that used a similar approach for analysis of NR data; this group compared NR data from a poly(*N*-isopropylacrylamide) brush with the predictions of a lattice SCF model.[37] However, in this previous study, the authors did not take into account the effects of the chain polydispersity, the roughness of the grafting surface, and the finite resolution of the NR measurement, all of which would significantly influence the calculation of expected reflectivity results. In the present work, we use a model that accurately takes these effects into account using parameters determined from independent data. Below, we explain the details of the SCF theory-based analysis procedure used in the present study:

(1) The first step was to compute the real-space density profile for the end-grafted PEO chains ($\phi_{\mathrm{PEO-water,SCF}}(z)$) using the continuum SCF formalism described in detail in our previous publications;[39−41] the SCF theory and equations used are also summarized briefly in section S1 of the Supporting Information. In this calculation, two parameters characterizing the interactions of PEO with other components of the system (i.e., water and PnBA) were used as adjustable parameters; one is the standard Flory−Huggins interaction parameter for the polymer−solvent (i.e., PEO−water) system ($\chi_{\mathrm{P-S}}$), and the other is the characteristic adsorption length (κ^{-1}) that characterizes the strength of the water-mediated interaction between the PEO polymer and the PnBA surface.[42,43] This latter parameter, κ^{-1}, appears in the boundary conditions for the SCF equations (eq S1.20 of section S1 of the Supporting Information), and its physical meaning becomes clear when it is considered that the product, $-\kappa b k_{\mathrm{B}}T$ (where b is the monomer size), represents the binding energy of a monomer to the surface at their contact distance ($z = 0$): for instance, the $\kappa^{-1} = 0$ condition (referred to as the hard-core repulsive condition) corresponds to the case where the grafting surface is nonpenetrable by the monomer; a finite positive value of κ^{-1} represents a situation in which the polymer segments have a binding affinity to the surface and produces an attractive boundary condition for the monomer distribution; when κ^{-1} goes to infinity, the wall does not impose any constraint on the distribution of the polymer segments at $z = 0$ (the grafting surface in this case is thus often described as being "indifferent"). It should also be pointed out that to be able to produce realistic segment density profiles for the end-grafted PEO chains, we had to take into account the molecular weight polydispersity of the PEO chains; for this purpose, the original PEO segment density profiles obtained by solving the SCF equations have been convoluted with a Schultz distribution[44] using an experimentally determined value of 1.07 for the polydispersity index of the PEO block;[19] see eqs S1.22−S1.24 of section S1 in the Supporting Information for details. The final outcome of this calculation is the volume fraction quantity denoted as $\phi_{\mathrm{PEO-water,SCF}}(z)$ in section S1 of the Supporting Information; see Figure S3 of the Supporting Information for sample $\phi_{\mathrm{PEO-water,SCF}}(z)$ profiles obtained under various κ^{-1} conditions.

(2) As discussed in section 3.2 (and also in refs 21, 24, and 28), the PnBA portion of the diblock copolymer chain spreads flat and assumes a (pseudo) 2D conformation on the water surface. Therefore, the conformation of the PnBA block cannot be modeled by the same 3D SCF theory used for the calculation of the PEO conformations, because the theory relies on the assumption that the conformation of the polymer to be modeled should not deviate much from the 3D Gaussian conformation (as can be seen from eq S1.2, Supporting Information). To deal with this issue, we developed a semiempirical approach to produce expected segment density profiles for the PnBA chains. This approach uses the electron density profiles ($\rho_{\mathrm{e}}(z)$) of the PEO−PnBA monolayer obtained previously from the multiple-box model analysis of the XR data,[36] to compute the PnBA segment density profiles for the air side of the PEO−PnBA monolayer ($\phi_{\mathrm{PnBA}}(z\leq 0)$); here, the $z = 0$ position is defined as the point where the function $\phi_{\mathrm{PnBA}}(z)$ is at its maximum. In this calculation, it is assumed that this upper surface of the PnBA domain in contact with air is free of water and PEO residues (i.e., $\phi_{\mathrm{D_2O}}(z\leq 0)$ and $\phi_{\mathrm{PEO}}(z\leq 0) = 0$). We also used the previous observation that the maximum electron density of the PnBA layer is identical to the value of the electron density of pure PnBA[36] (that is, $\phi_{\mathrm{PnBA}}(z) = 1$ at $z = 0$). Note that the $\phi_{\mathrm{PnBA}}(z\leq 0)$ profiles were calculated using the XR fit results (rather than from the NR data), because the PnBA−air interface makes a dominant contribution to the XR from the PEO−PnBA monolayer, whereas it only weakly contributes to the NR signal; this can be seen from the comparison of the values of the relative contrast factors, $\rho_{\mathrm{e,PnBA}}/\rho_{\mathrm{e,H_2O}}$ (=1.10) ≫ $\mathrm{SLD_{PnBA}}/\mathrm{SLD_{D_2O}}$ (=0.108). The PnBA−water interfacial profile ($\phi_{\mathrm{PnBA}}(z>0)$) was obtained by assuming a half-Gaussian shape for the profile; the width of the half-Gaussian was adjusted such that the mass balance for PnBA is closed: $\int_{-\infty}^{\infty}\phi_{\mathrm{PnBA}}(z)\,\mathrm{d}z\cdot\rho_{\mathrm{PnBA}} = M_{\mathrm{PnBA}}/(\alpha\cdot N_{\mathrm{Av}})$ where ρ_{PnBA} and M_{PnBA} denote the mass density of PnBA and the molar mass of the PnBA block, respectively, and N_{Av} is Avogadro's number. A sample $\phi_{\mathrm{PnBA}}(z)$ profile thus obtained is shown in Figure S4 of the Supporting Information; the resulting PnBA

dx.doi.org/10.1021/jp301817e | J. Phys. Chem. B 2012, 116, 7367−7378

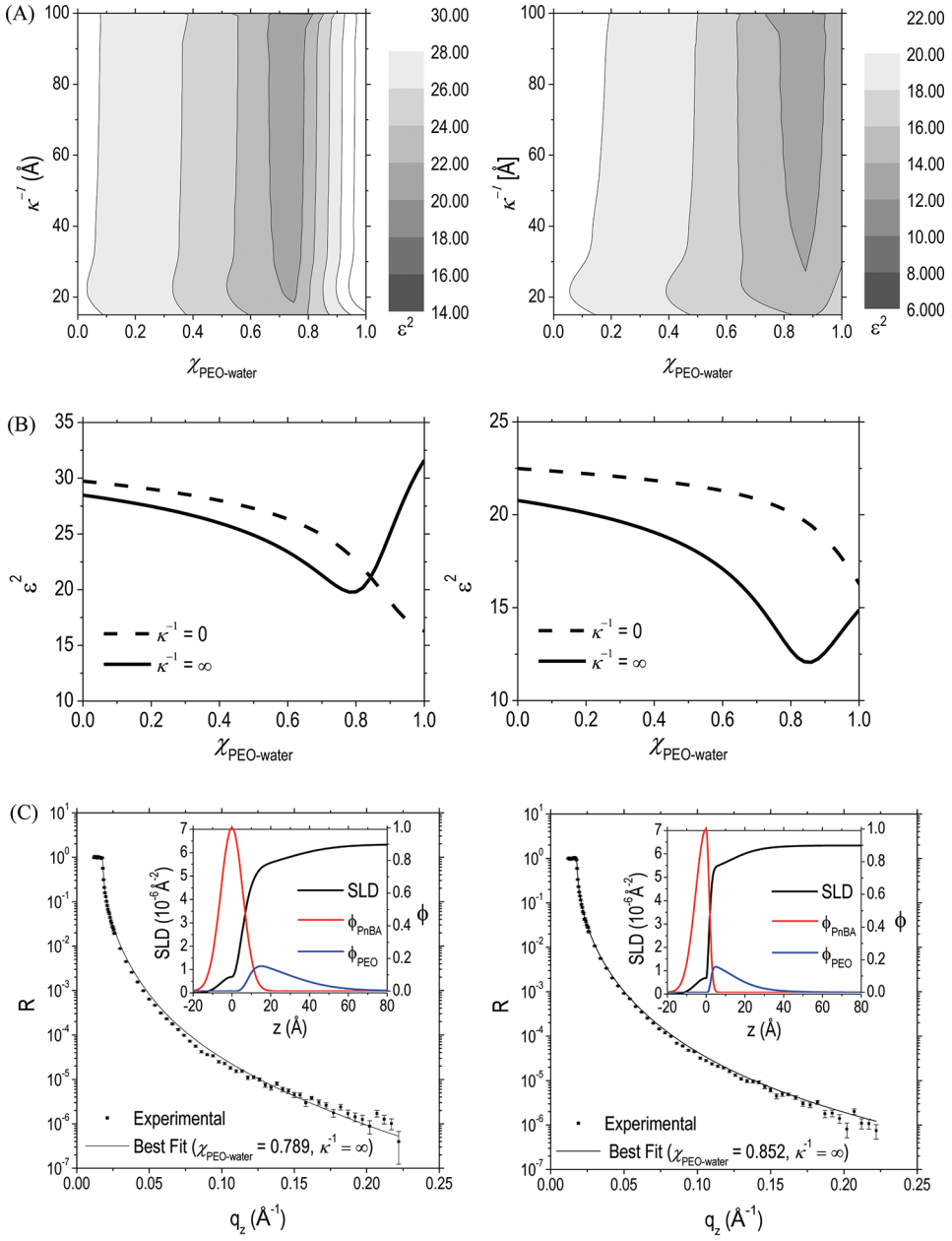

Figure 3. Results of the SCF theory-based analysis of the NR data obtained from the PEO−PnBA monolayer at two different area per chain conditions: α = 1350 (left) and 2200 (right) Å^2/chain. (A) Contour plots of the sum of the error square (ε^2) as a function of the two adjustable parameters, the Flory−Huggins interaction parameter ($\chi_{PEO-water}$), and the characteristic adsorption length (κ^{-1}). (B) Plots of ε^2 vs $\chi_{PEO-water}$ at two representative values of κ^{-1}, i.e., $\kappa^{-1} = 0$ (representing the hard-core repulsive condition at the grafting surface) and $\kappa^{-1} = \infty$ (representing the indifferent character of the grafting surface). (C) Experimental NR data shown as points with error bars. The solid curves were produced on the basis of the best-fit parameters ($\chi_{PEO-water}$ = 0.789 and $\kappa^{-1} = \infty$ at α = 1350 Å^2/chain, and $\chi_{PEO-water}$ = 0.852 and $\kappa^{-1} = \infty$ at α = 2200 Å^2/chain).

layer parameters at several different α values are also presented in Table S1 (Supporting Information). As can be seen from the sample PnBA distribution, the PnBA film has a finite roughness. An important consequence of this property is that even if we assume that all the junction points between the PEO and PnBA blocks are located strictly at the PnBA−water interface, because the distribution of the positions of the PnBA−water interface has a finite spread in location along the z-axis, the z-positions of the grafting points of the PEO brush chains (i.e., the block junction points) are also accordingly diffusely distributed over $z > 0$. Therefore, the PEO segment density distribution becomes further widened when considered with respect to an absolute frame of reference in position. To take this interfacial smearing effect into account, we first defined an unnormalized probability function describing the statistical distribution of the locations of the PEO grafting points:

$$P_{\text{junction}}(z) = \begin{cases} 0 & (\text{for } z < 0) \\ \phi_{\text{PnBA}}(z)\cdot[1 - \phi_{\text{PnBA}}(z)] & (\text{for } z \geq 0) \end{cases} \quad (1)$$

Then, we once again convoluted the PEO distribution function obtained in step 1 (i.e., $\phi_{\text{PEO-water,SCF}}(z)$) with the junction-point distribution function $P_{\text{junction}}(z)$ to obtain the final form of the function describing the distribution of the PEO segments in the aqueous phase $\phi_{\text{PEO-water}}(z)$:

dx.doi.org/10.1021/jp301817e | J. Phys. Chem. B 2012, 116, 7367−7378

$$\phi_{\mathrm{PEO-water}}(z) = \frac{\int_{-\infty}^{\infty} \phi_{\mathrm{PEO-water,SCF}}(z - z')\, P_{\mathrm{junction}}(z')\, \mathrm{d}z'}{\int_{-\infty}^{\infty} P_{\mathrm{junction}}(z')\, \mathrm{d}z'} \tag{2}$$

Note that $\phi_{\mathrm{PEO-water}}(z)$ is the volume fraction of PEO in the aqueous phase excluding the volume occupied by PnBA. Afterward, we calculated the volume fractions of PEO, D_2O, and air in the total system using the following equations

$$\phi_{\mathrm{PEO}}(z) = \begin{cases} 0 & (\text{for } z < 0) \\ [1 - \phi_{\mathrm{PnBA}}(z)][\phi_{\mathrm{PEO-water}}(z)] & (\text{for } z \geq 0) \end{cases}$$

$$\phi_{\mathrm{D_2O}}(z) = \begin{cases} 0 & (\text{for } z < 0) \\ [1 - \phi_{\mathrm{PnBA}}(z)][1 - \phi_{\mathrm{PEO-water}}(z)] & (\text{for } z \geq 0) \end{cases}$$

$$\phi_{\mathrm{air}}(z) = \begin{cases} 1 - \phi_{\mathrm{PnBA}}(z) & (\text{for } z < 0) \\ 0 & (\text{for } z \geq 0) \end{cases} \tag{3}$$

Note that the volume fractions of the individual components satisfy the constraint

$$\phi_{\mathrm{PnBA}}(z) + \phi_{\mathrm{PEO}}(z) + \phi_{\mathrm{D_2O}}(z) + \phi_{\mathrm{air}}(z) = 1 \tag{4}$$

Finally, the overall scattering length density ($\mathrm{SLD}(z)$) profile was estimated by

$$\mathrm{SLD}(z) = \mathrm{SLD}_{\mathrm{PnBA}} \cdot \phi_{\mathrm{PnBA}}(z) + \mathrm{SLD}_{\mathrm{PEO}} \cdot \phi_{\mathrm{PEO}}(z) + \mathrm{SLD}_{\mathrm{D_2O}} \cdot \phi_{\mathrm{D_2O}}(z) + \mathrm{SLD}_{\mathrm{air}} \cdot \phi_{\mathrm{air}}(z) \tag{5}$$

Note that here air is considered as void, and thus $\mathrm{SLD}_{\mathrm{air}} = 0$. See Figure 3C for real examples of $\phi_{\mathrm{PnBA}}(z)$, $\phi_{\mathrm{PEO}}(z)$, and $\mathrm{SLD}(z)$ profiles.

(3) From the scattering length density profile, we calculated the spatially varying neutron refractive index of the monolayer system (assuming negligible absorption of the neutron radiation by the sample):

$$n(z) = 1 - \left(\frac{\lambda^2}{2\pi}\right)\mathrm{SLD}(z) \tag{6}$$

where λ is the wavelength of the neutron radiation used (=4.760 Å). This information on the position-dependent refractive index of the brush system was then converted to the reflected neutron intensity profile in reciprocal space ($R(q_z)$) by using the establish procedure known as the dynamic transfer-matrix method; a summary of the procedure used in this calculation is given in section S2 of the Supporting Information, and a detailed discussion of the transfer matrix method can be found, for example, in ref 45. For quantitative comparison between the predicted and observed reflectivities, it was also necessary to take into account the effect of the finite q_z resolution of the NR measurement. For this purpose, the predicted reflectivity profile $R(q_z)$ was further convoluted with an NR instrument resolution function $P(q_z, q'_z)$ using the approach proposed in ref 46:

$$\langle R(q_z)\rangle = \int_0^{\infty} R(q'_z)\, P(q_z, q'_z)\, \mathrm{d}q'_z \tag{7}$$

$$P(q_z, q'_z) = \frac{1}{\sqrt{2\pi}\,\sigma_{\mathrm{res+-}}(q'_z)} \exp\left[-\frac{1}{2}\left(\frac{q_z - q'_z}{\sigma_{\mathrm{res+-}}(q'_z)}\right)^2\right] \tag{8}$$

$$\sigma_{\mathrm{res+-}}(q'_z) = \frac{\left\{2\left[\sigma_x\left(\frac{4\pi}{\lambda}\cos\theta\,\tan\theta_{\mathrm{mon}} - q'_z\right)\right]^2 + (q'_z\eta D)^2\right\}^{1/2}}{D\,\tan\theta_{\mathrm{mon}}} \tag{9}$$

where σ_x is the variance of the Gaussian neutron transmission function ($\sigma_x = W/(12)^{1/2}$ where W is the width of the slits), θ is the reflection angle, which is related to the momentum transfer vector by $q'_z = (4\pi/\lambda)\sin\theta$, θ_{mon} is the diffraction angle of the monochromator, η is the variance of the Gaussian distribution for the orientations of the crystallites of the monochromator crystals ($\eta = \mathrm{fwhm}_{\mathrm{mosaic}}/(2(2\ln 2))^{1/2}$ where $\mathrm{fwhm}_{\mathrm{mosaic}}$ is the full width at half-maximum of the orientation spread), D is the distance between the slits, and the subscript "+−" in the "$\sigma_{\mathrm{res+-}}$" notation for the variance of the resolution function reflects the so-called "+−" reflection geometry of the sample with respect to the monochromator used in the NR measurements.

(4) With the procedures outlined in steps 1−3 above, expected reflectivity profiles ($\langle R(q_z)\rangle$) were calculated for systematically varying combinations of $\chi_{\mathrm{PEO-water}}$ and κ^{-1} values and were compared with the experimental NR data ($R_{\mathrm{exp}}(q_z)$). For each prediction, the sum of the error squared (ε^2) was calculated, and this quantity was used as the objective function to be minimized in search of the best-fit values of the parameters. The ε^2 values were evaluated in the log scale to be consistent with the visual presentations of the comparison results (presented in Figure 3C):

$$\varepsilon^2 = \sum_i^{\mathrm{all}} \left[\frac{\log(\langle R(q_{z,i})\rangle) - \log(R_{\mathrm{exp}}(q_{z,i}))}{\log(R_{\mathrm{exp}}(q_{z,i}) + \Delta R^{+}_{\mathrm{exp}}(q_{z,i})) - \log(R_{\mathrm{exp}}(q_{z,i}) - \Delta R^{-}_{\mathrm{exp}}(q_{z,i}))}\right]^2 \tag{10}$$

Using the above procedures, we analyzed the diblock NR data. Specifically, in the present work we focused our analysis on the data obtained at the two lowest area-per-chain values (α = 1350 and 2200 Å^2/chain). Under these α conditions, it can be guaranteed that the grafted PEO chains sufficiently laterally overlap one another (i.e., $\alpha/\pi R_{\mathrm{G,PEO(3D)}}{}^2 < \sim 1$ as shown in Figure 2A) and thus are truly in the polymer brush regime. This situation also enables us to simplify the SCF computation in step 1 by one-dimensionalization of the problem. The results of the SCF theory-based analysis of the two sets of NR data are demonstrated in Figure 3A. In this figure, we present contour plots of the fit quality measure (ε^2) as a function of the two adjustable parameters, $\chi_{\mathrm{PEO-water}}$ (shown in the x-axis) and κ^{-1} (y-axis). As shown in the figure, consistently between the two area-per-chain conditions examined, we found that the best-fit prediction was obtained near the high $\chi_{\mathrm{PEO-water}}$ and κ^{-1} corner of the plot within the parameter ranges demonstrated, $\chi_{\mathrm{PEO-water}}$ = 0−1.0, and κ^{-1} = 0−100 Å; it should be noted that the $\chi_{\mathrm{PEO-water}}$ range examined was chosen on the basis of the prediction that (as will be shown later in Figure 5) when $\chi_{\mathrm{PEO-water}} > \sim 0.9$ the lateral pressure of the PEO brush becomes negative, which contradicts what was observed experimentally (section 3.4). The exact values of the fit parameters that gave the least errors in simulating the experimental data are $\chi_{\mathrm{PEO-water}} = 0.789$ and $\kappa^{-1} = \infty$ at α = 1350 Å^2 per chain, and $\chi_{\mathrm{PEO-water}} = 0.852$ and $\kappa^{-1} = \infty$ at α = 2200 Å^2 per chain.

We note that the best-fit condition of κ^{-1} (=∞) is realized when κ^{-1} goes to infinity, which means that the derivative of the

dx.doi.org/10.1021/jp301817e | J. Phys. Chem. B 2012, 116, 7367−7378

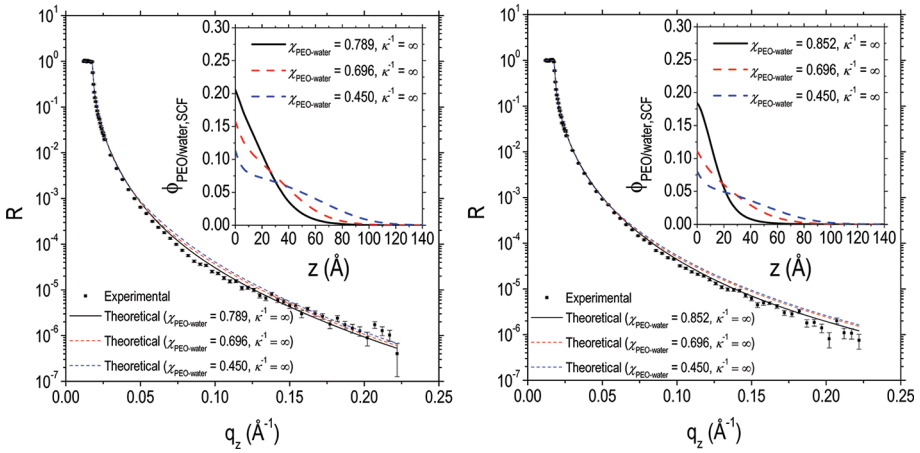

Figure 4. Plots demonstrating the sensitivity of the model prediction for NR reflectivity to the variation of the $\chi_{PEO-water}$ parameter. κ^{-1} was set at the best-fit value ($\kappa^{-1} = \infty$). The analysis was conducted with the data obtained at two different area per chain conditions: α = 1350 (left) and 2200 (right) Å^2/chain.

$\phi_{PEO-water,SCF}(z)$ curve at $z = 0$ is equal to zero. As shown in Figure 3B, we have also confirmed that the hard-core repulsive (i.e., $\kappa^{-1} = 0$) boundary condition does not provide better estimates of the reflectivity profiles for the range of $\chi_{PEO-water}$ values considered reasonable (i.e., $\chi_{PEO-water} < \sim 0.9$, as discussed in the previous paragraph). Therefore, it is concluded that the PnBA−water interface (to which the PEO chains are grafted) acts on PEO neither attractively nor repulsively and minimally influences the distributions of the PEO segments (therefore, the grafting surface can be described as being "indifferent"). This result is fully consistent with the observation that addition of PEO into the water subphase does not cause a change in the surface pressure property of a PnBA monolayer preformed at the air−water interface (discussed in section 3.1).

The best-fit $\chi_{PEO-water}$ values (where the errors were minimized) were found to be 0.789 ± 0.066 (at α = 1350 Å^2/chain) and 0.852 ± 0.051 (at α = 2200 Å^2/chain), which are significantly greater than the $\chi_{PEO-water}$ values documented in the literature for PEO in bulk water (≈0.45 at 20 °C);[11] note here that the uncertainty of $\chi_{PEO-water}$ was defined (arbitrarily) to represent the range of $\chi_{PEO-water}$ values in which ε^2 deviates by less than 5% from the minimum value. As shown in Figure 3C, the model's fit quality under the best-fitting parameter estimates was satisfactory over the entire range of q_z examined, which supports the reasonableness of the estimated parameters; we note that at intermediate q_z values there are very minor deviations of the model predictions from the experimental NR data that might be attributed to the reduced water density in the PEO brush,[36] which is not considered in the SCF model. It should also be pointed out that it would not be too accurate to deduce, simply on the basis of the result $\chi_{PEO-water} > 1/2$, that the grafted PEO chains indeed experience an unfavorable ("poor") solvent environment and are thus describable as hydrophobic. We raise this point because the physical assumptions used in the present SCF model are not identical to those of the Flory−Huggins theory from which the $\chi_{P-S} = 1/2$ criterion for distinction between the "good" and "poor" solvent conditions has been originally derived. For instance, in our SCF model we used a monomer volume that is different from the value of the solvent volume used (i.e., v_{PEO} = 59.2 Å^3 and v_{water} = 29.9 Å^3). For this reason alone, simply setting the $\chi_{PEO-water}$ value to 0.5 in our model, for example, would not be able to produce results that precisely correspond to the behavior under the so-called θ condition. To be able to draw a solid conclusion regarding the disfavored (or favorable) nature of the measured value of the PEO−water interaction parameter, we conducted an additional test as follows. We considered a single PEO chain dissolved in water in its free (ungrafted) state. We fixed one end of the chain to the origin of the simulation box and calculated the radial distribution of the position of the other end using the SCF model at four different values of $\chi_{PEO-water}$ (0.20, 0.50, 0.696, and 0.80). In Figure S5 (Supporting Information), the results of these calculations are presented in comparison with the end-to-end distance probability distribution function of a Gaussian chain of the same molecular weight. It is first notable that the SCF prediction for $\chi_{PEO-water}$ = 0.50 does not match the Gaussian behavior; the Gaussian statistics was precisely reproduced when $\chi_{PEO-water}$ is set to about 0.696. Nonetheless, at $\chi_{PEO-water}$ = 0.80 the PEO chain is seen to be significantly shrunk with respect to its Gaussian conformation. It is thus obvious that the $\chi_{PEO-water}$ = 0.80 condition should be categorized as a poor solvent situation, and the conclusion of the NR analysis should be that PEO chains are not hydrophilic when they exist as polymer brush chains. It is notable that the difference by which the value of $\chi_{PEO-water}$ for the PEO brush system is estimated to be greater than that corresponding to the θ condition (i.e., $\chi_{PEO-water}$(brush chains)/$\chi_{PEO-water}$(θ condition) ≈ 1.2) is consistent with the known range of concentration-dependent variation of the $\chi_{PEO-water}$ parameter.[47]

3.4. Discussion of the Parametric Sensitivity and the Consistency between the Neutron Reflectivity and Surface Pressure−Area Isotherm Results. One might question whether the uncertainties associated with the best-fit values of the $\chi_{PEO-water}$ parameter are sufficiently small to be able to draw the above-stated conclusion. To confirm this point, we examined the parametric sensitivity of the model predictions with respect to variations of $\chi_{PEO-water}$ under a fixed value of κ^{-1} (= ∞). In Figure 4, we present plots that illustrate that a decrease of the $\chi_{PEO-water}$ parameters from its best-fit values ($\chi_{PEO-water}$ = 0.789 at α = 1350 Å^2/chain, and $\chi_{PEO-water}$ = 0.852 at α = 2200 Å^2/chain) to the value that would yield a Gaussian segment distribution for a free PEO chain (i.e., $\chi_{PEO-water} \approx 0.696$ from Figure S5, Supporting Information) causes significant deviations of the model predictions from the measurements (beyond the estimated measurement errors). This results demonstrate that

dx.doi.org/10.1021/jp301817e | J. Phys. Chem. B 2012, 116, 7367−7378

the conclusion that for the grafted PEO chains water becomes a poor solvent is statistically significant.

Another point that we also clarify concerns the question: If indeed the grafted PEO chains are in an unfavorable solvent environment, why does the brush layer resist lateral compression and exhibit positive (instead of negative) surface pressures (see Figure 2A)? Or even, why are PEO brushes, in general, so effective in protecting the surfaces (or particles), to which they are end-grafted, from aggregation (rather than causing it by bridging forces)? The answer to these questions lies (at least partly) in the fact that the hydrophobicity of the PEO brush chains (considered in the SCF model in eq S1.3) is rather marginal, and insufficient to overcome the other opposing force of the chain conformational entropy (as modeled through eq S1.2 in section S1 of the Supporting Information). To demonstrate this point, we conducted SCF calculations of the values of the surface pressure produced by the lateral interchain interactions between the end-grafted PEO chains under various surface concentrations of PEO ($1/\alpha$) at various $\chi_{PEO-water}$ values (0.696, 0.789, 0.852, 0.950, 1.000), and $\kappa^{-1} = \infty$. Briefly, we first computed the total free energy of the brush system (F) using eq S1.7 in section S1 of the Supporting Information and then the surface pressure quantity (Π) using eq S1.26 (Supporting Information). The resultant Π values obtained as a function of α were compared with a fictitious isotherm curve of the PEO brush layer obtained by subtracting the rescaled Π vs α plot of the PnBA homopolymer from the $\Pi-\alpha$ isotherm of the PEO−PnBA diblock copolymer (both displayed in Figure 2A), i.e., $\Pi_{PEO}(\alpha) \equiv \Pi_{PEO-PnBA}(\alpha) - \Pi_{PnBA(rescaled)}(\alpha)$; note that this calculation assumes that at $\alpha \approx \alpha_o$ (=2190 Å^2/chain) and the lateral pressure of the PEO brush is negligible (i.e., $\Pi_{PEO} \approx 0$), which is reasonable because at this α condition the normalized area per chain value, $\alpha/\pi R_{G,PEO(3D)}^2$, is greater than unity (as can be seen from Figure 2A). The results of this investigation are presented in Figure 5. As shown in the figure, when $\chi_{PEO-water}$ is sufficiently

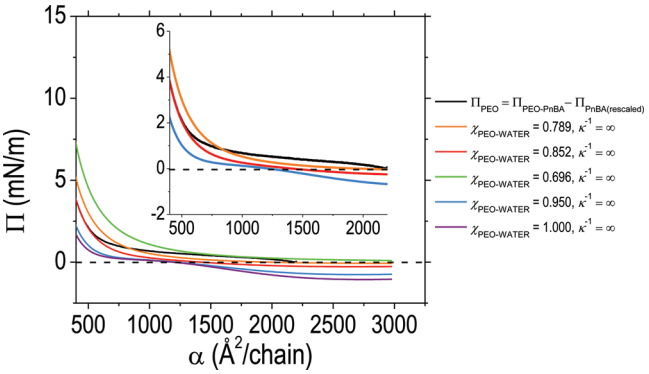

Figure 5. Experimental surface pressure−area isotherm data for the PEO brush layer (black curve), in comparison with the surface pressure profiles calculated using the SCF theory at five different values of $\chi_{PEO-water}$ (other colors). The inset is a magnified view of the same plot in the low-to-intermediate-α region produced with a fewer number of data lines for clarity.

high, the surface pressure of the PEO brush is estimated to be significantly negative over a wide range of α (e.g., when $\chi_{PEO-water}$ = 0.950, $\Pi_{PEO} \approx -0.68$ mN/m at α = 2200 Å^2/chain). At the best-fit parameter set (i.e., $\chi_{PEO-water}$ = 0.789 (or 0.852), and $\kappa^{-1} = \infty$), however, the PEO brush pressure was confirmed to be largely positive for the reason explained above. Further, the predicted values of Π_{PEO}, obtained at this condition with no additional adjustable parameters, are in reasonable agreement with the experimental data, which indicates that the results obtained from the analysis of the NR data are also consistent with the surface pressure−area isotherm results.

4. CONCLUSION

A model poly(ethylene oxide) (PEO) brush system, prepared by spreading a poly(ethylene oxide)−poly(*n*-butyl acrylate) (PEO−PnBA) amphiphilic diblock copolymer onto an air−water interface, was investigated by using a combined experimental and theoretical approach (that includes combined experimental techniques of surface pressure−area isotherm and neutron reflectivity (NR) measurements and self-consistent field (SCF) theoretical studies). We attempted to answer two important questions concerning the thermodynamic properties of PEO brushes under the influence of the (posited) *n*-cluster interactions:

(1) Can it be demonstrated that PEO chains are indeed *not hydrophilic* when they exist as polymer brush chains (or can we show that $\chi_{PEO-water} > 1/2$)?
(2) If indeed the grafted PEO chains are in a poor solvent environment, would the brush layer favor lateral compression and exhibit negative surface pressures?

From the study, we were able to draw the following conclusions regarding the above questions:

(1) PEO chains are indeed *nonhydrophilic* when they are arranged in the polymer brush configuration; that is, the value of $\chi_{PEO-water}$ was measured to be significantly greater than that corresponding to the θ condition in Flory−Huggins solutions.
(2) However, even though the grafted PEO chains experience a poor solvent environment, the PEO brush layer exhibits positive surface pressures, because the hydrophobicity of the PEO brush chains (which favors compression) is insufficient to overcome the opposing force of the chain conformational entropy (which resists compression).

■ ASSOCIATED CONTENT

Supporting Information

The numerical SCF theory (section S1); the dynamic transfer-matrix method for the calculation of reflectivity curves (section S2); the roughness properties of the air−water monolayer formed by the PnBA block of the PEO−PnBA polymer (Table S1); a representative liquid AFM image of the LB-deposited PEO−PnBA film (Figure S1); NR profile from pure D_2O (Figure S2); sample $\phi_{PEO-water,SCF}(z)$ profiles under various κ^{-1} conditions at a fixed value of $\chi_{PEO-water}$ (Figure S3); the volume fraction profiles of the PEO and PnBA monomers, water, and air calculated using the best-fit parameter estimates (Figure S4); the radial end-to-end distance distribution functions for a free PEO chain calculated using the SCF model for several different combinations of ν_{PEO}, ν_{water} and $\chi_{PEO-water}$ values (Figure S5). This information is available free of charge via the Internet at http://pubs.acs.org.

■ AUTHOR INFORMATION

Corresponding Author

*E-mail: yywon@ecn.purdue.edu.

Notes

The authors declare no competing financial interest.

■ ACKNOWLEDGMENTS

We thank the National Science Foundation (NSF) for providing financial support of this research (DMR-0906567).

■ REFERENCES

(1) Harris, M. *Poly(ethylene glycol) chemistry: biotechnical and biomedical applications*, 1st ed.; Springer: Berlin, 1992.
(2) McPherson, T.; Kidane, A.; Szleifer, I.; Park, K. *Langmuir* **1998**, *14*, 176.
(3) Smart, T. P.; Mykhaylyk, O. O.; Ryan, A. J.; Battaglia, G. *Soft Matter* **2009**, *5*, 3607.
(4) Wesemann, A.; Ahrens, H.; Steitz, R.; Forster, S.; Helm, C. A. *Langmuir* **2003**, *19*, 709.
(5) Won, Y.-Y.; Davis, H. T.; Bates, F. S.; Agamalian, M.; Wignall, G. D. *J. Phys. Chem. B* **2000**, *104*, 7134.
(6) Zheng, Y.; Won, Y. Y.; Bates, F. S.; Davis, H. T.; Scriven, L. E.; Talmon, Y. J. *Phys. Chem. B* **1999**, *103*, 10331.
(7) Won, Y.-Y.; Bates, F. S. Nonionic Block Copolymer Wormlike Micelles. In *Giant Micelles: Properties and Applications*; Zana, R., Kaler, E. W., Eds.; CRC Press/Taylor & Francis: Boca Raton, FL, 2007.
(8) Connor, T. M.; McLauchlan, K. A. *J. Phys. Chem.* **1965**, *69*, 1888.
(9) Tasaki, K. *J. Am. Chem. Soc.* **1996**, *118*, 8459.
(10) Baulin, V. A.; Halperin, A. *Macromolecules* **2002**, *35*, 6432.
(11) Venohr, H.; Fraaije, V.; Strunk, H.; Borchard, W. *Eur. Polym. J.* **1998**, *34*, 723.
(12) Hammouda, B.; Ho, D. L.; Kline, S. *Macromolecules* **2004**, *37*, 6932.
(13) De Gennes, P. G. C.R. *Acad. Sci. Paris Ser. II* **1991**, 313.
(14) Halperin, A. *Eur. Phys. J. B* **1998**, *3*, 359.
(15) Wagner, M.; Brochard-Wyart, F.; Hervet, H.; de Gennes, P. *Colloid Polym. Sci.* **1993**, *271*, 621.
(16) Hu, T.; Wu, C. *Phys. Rev. Lett.* **1999**, *83*, 4105.
(17) Bartlett, D. W.; Davis, M. E. *Bioconjugate Chem.* **2007**, *18*, 456.
(18) Gary, D. J.; Lee, H.; Sharma, R.; Lee, J.-S.; Kim, Y.; Cui, Z. Y.; Jia, D.; Bowman, V. D.; Chipman, P. R.; Wan, L.; Zou, Y.; Mao, G.; Park, K.; Herbert, B.-S.; Konieczny, S. F.; Won, Y.-Y. *ACS Nano* **2011**, *5*, 3493.
(19) Sharma, R.; Goyal, A.; Caruthers, J. M.; Won, Y.-Y. *Macromolecules* **2006**, *39*, 4680.
(20) Sharma, R.; Lee, J.-S.; Bettencourt, R. C.; Xiao, C.; Konieczny, S. F.; Won, Y.-Y. *Biomacromolecules* **2008**, *9*, 3294.
(21) Witte, K. N.; Kewalramani, S.; Kuzmenko, I.; Sun, W.; Fukuto, M.; Won, Y.-Y. *Macromolecules* **2010**, *43*, 2990.
(22) Kienzle, P. A.; K. V. O. D., Ankner, J. F.; Berk, N. F.; C. F. Majkrzak. *REFLPAK*; NCNR: 2000−2006.
(23) Baulin, V. A.; Zhulina, E. B.; Halperin, A. *J. Chem. Phys.* **2003**, *119*, 10977.
(24) Witte, K. N.; Hur, J.; Sun, W.; Kim, S.; Won, Y.-Y. *Macromolecules* **2008**, *41*, 8960.
(25) Cox, J. K.; Yu, K.; Constantine, B.; Eisenberg, A.; Lennox, R. B. *Langmuir* **1999**, *15*, 7714.
(26) Kumaki, J. *Macromolecules* **1988**, *21*, 749.
(27) *Handbook of Common Polymers: Fibres, Films, Plastics, and Rubbers*; Roff, W. J., Ed.; CRC Press: Cleveland, OH, 1971.
(28) Hur, J.; Witte, K. N.; Sun, W.; Won, Y. Y. *Langmuir* **2010**, *26*, 2021.
(29) Cao, B. H.; Kim, M. W. *Faraday Discuss.* **1994**, *98*, 245.
(30) Faure, M. C.; Bassereau, P.; Carignano, M. A.; Szleifer, I.; Gallot, Y.; Andelman, D. *Eur. Phys. J. B* **1998**, *3*, 365.
(31) Hiemenz, P. C.; Lodge, T. P. *Polymer Chemistry*, 2nd ed.; CRC Press: Boca Raton, FL, 2007.
(32) Brandrup, J.; Immergut, E. H.; Grulke, E. A.; Abe, A.; Bloch, D. R. *Polymer Handbook*, 4th ed.; John Wiley & Sons: New York, 1999.
(33) Doi, M.; Edwards, S. F. *The Theory of Polymer Dynamics*; Oxford University Press Inc: New York, 1986.
(34) Fleer, G. J.; Cohen Stuart, M. A.; Scheutjens, J. M. H. M.; Cosgrove, T.; Vincent, B. *Polymers at Interfaces*; Chapman & Hall: New York, NY, 1993.
(35) Kawaguchi, S.; Imai, G.; Suzuki, J.; Miyahara, A.; Kitano, T. *Polymer* **1997**, *38*, 2885.
(36) Lee, H.; Kim, D. H.; Park, H.-W.; Mahynski, N. A.; Kim, K.; Meron, M.; Lin, B.; Won, Y.-Y. *J. Phys. Chem. Lett* **2012**, accepted (DOI: 10.1021/jz3002772).
(37) Zhang, J. M.; Nylander, T.; Campbell, R. A.; Rennie, A. R.; Zauscher, S.; Linse, P. *Soft Matter* **2008**, *4*, 500.
(38) Schlossman, M. L.; Pershan, P. S. X-ray and Neutron Scattering from Liquid Surfaces. In *Light Scattering by Liquid Surfaces and Complementary Techniques*; Langevin, D., Ed.; Marcel Dekker: New York, 1992.
(39) Witte, K. N.; Kim, S.; Won, Y.-Y. *J. Phys. Chem. B* **2009**, *113*, 11076.
(40) Witte, K. N.; Won, Y.-Y. *Macromolecules* **2006**, *39*, 7757.
(41) Witte, K. N.; Won, Y.-Y. *Macromolecules* **2008**, *41*, 2735.
(42) Wang, Q. *Macromolecules* **2005**, *38*, 8911.
(43) De Gennes, P. G. *Scaling Concepts in Polymer Physics*; Cornell University Press: Ithaca, NY, 1979.
(44) Sides, S. W.; Fredrickson, G. H. *J. Chem. Phys.* **2004**, *121*, 4974.
(45) Daillant, J.; Gibaud, A. Specular Reflectivity from Smooth and Rough Surfaces. In *X-Ray and Neutron Reflectivity: Principles and Applications: Principles and Applications*; Daillant, J., Gibaud, A., Eds.; Springer: Berlin, 1999.
(46) Bouwman, W. G.; Pedersen, J. S. *J. Appl. Crystallogr.* **1996**, *29*, 152.
(47) Franks, F. *Water*; Royal Society of Chemistry: London, 1984; Vol. *4*.
(48) NIST. *Neutron scattering lengths and cross sections*; http://www.ncnr.nist.gov/resources/n-lengths/.
(49) Wunderlich, B. Macromolecular Physics. *Crystal Structure,Morphology, and Defects*; Academic Press: New York, 1973; Vol. *1*.

■ NOTE ADDED AFTER ASAP PUBLICATION

This paper was published ASAP on June 4, 2012. Figures 3C and 4 were transposed. The revised paper was reposted on June 7, 2012.